RESEARCH ARTICLE
SOLAR PHYSICS

Earth and Planetary Physics
9: 752–759, 2025
doi: 10.26464/epp2025061

Analysis for the results of geomagnetic storms measured by Macau Science Satellite-1

HaiSheng Ji[1,2*], Dong Li[1*], HongBo Yao[3], JianPing Li[2], and YanJie Zhang[1]

[1]Purple Mountain Observatory, Chinese Academy of Sciences, Nanjing 210023, China;

[2]Xinjiang Astronomical Observatory, Chinese Academy of Sciences, Ürümqi 830011, China;

[3]Macau Institute of Space Technology and Application, Macau University of Science and Technology, Macao 999078, China

Key Points:

- We carried out coordinated data analysis combining observations of soft X-ray (SXR) and vector magnetic field by Macau Science Satellite-1 (MSS-1) with other facilities in space during a series of X-class flares in October, 2024.
- The magnetic fields measured by MSS-1, especially its external (e_1^0) coefficient, can well be used for monitoring the geomagnetic disturbance.
- The results confirms that, in addition to flare class, longer duration of a flare represents sustained action on the coronal mass ejection and solar wind.

Citation: Ji, H. S., Li, D., Yao, H. B., Li, J. P., and Zhang, Y. J. (2025). Analysis for the results of geomagnetic storms measured by Macau Science Satellite-1. *Earth Planet. Phys.*, *9*(3), 752–759. http://doi.org/10.26464/epp2025061

Abstract: Strong flares and/or coronal mass ejections (CMEs) could bring us disastrous space weather, destroy crucial technology in space, and cause a large-scale blackout during some extreme cases. They frequently cause geomagnetic storms, which is a sudden disturbance of the Earth's magnetosphere. It is well accepted that CMEs play a dominant role in causing geomagnetic storms by a direct impact, but it is still not very clear regarding their association with solar flares. The association would be helpful for forecasting geomagnetic storms directly from flares, which are much easier to observe. The Macau Science Satellite-1 (MSS-1) mission, with the scientific aim of studying the origin and evolution of the geomagnetic field, is able to accurately measure the vector geomagnetic field. Besides, it measures rapid spectral evolution of the solar X-ray irradiance of solar flares. In this study, we analyzed measurements by MSS-1 during a series of X-class flares in October of 2024, and saw the relationship between the flares and the associated geomagnetic storms. The observations support that the major geomagnetic storms tend to be associated with flares' duration in addition to flare class. We also find that long duration ones have radiated more energy in the extreme ultraviolet waveband. Being equally important, our results show that the magnetic fields measured by MSS-1, especially its external (e_1^0) coefficient, can well be used for monitoring the geomagnetic disturbance.

Keywords: Macau Science Satellite-1 (MSS-1); solar flares; geomagnetic storms

1. Introduction

Solar flares are impulsive and explosive processes of energy releases through the magnetic reconnection, and they can be simultaneously observed in multi-height atmospheres on the Sun (Benz, 2017). The released energies are mostly converted from the free magnetic energy that is stored in nonpotential magnetic fields, which are overlaid on the current-carrying fields and characterized by complex magnetic geometries (e.g., Priest and Forbes, 2002; Warmuth and Mann, 2016; Li J et al., 2021; Yan X et al., 2022; Lu ZK et al., 2024). Solar flares are thought to be the most intense events in our solar system, and they can release the energy as high as ~10^{32} erg in a short timescale of minutes. They are regarded as the very initial source of space weather via radiation, compared with coronal mass ejections (CMEs), solar energetic particles (SEPs), and solar wind disturbances (Raouafi and Vourlidas, 2021). Besides, not all flares are associated with CMEs.

Geomagnetic storms are major and rapid variations of the Earth's magnetosphere, and they often occur when there are very efficient and dramatic exchanges of energies from the interplanetary space surrounding the Earth (Gonzalez et al., 1994). The geomagnetic storm may be directly caused by CMEs, and then it could lead to great changes in plasmas, fields, or currents in the Earth's magnetosphere, resulting in serious influences on human activities with high technology (Lakhina and Tsurutani, 2016; Pulkkinen et al., 2017). Severe geomagnetic storms can even cause the disruption of electrical systems, navigation problems, satellite damages, and communication failures (e.g., Cliver and Svalgaard, 2004; Meng X et al., 2019; Hayakawa et al., 2021).

Correspondence to: H. S. Ji, jihs@pmo.ac.cn
D. Li, lidong@pmo.ac.cn
Received 30 MAR 2025; Accepted 14 APR 2025.
First Published online 25 APR 2025.

The geomagnetic storms may be effectively created on the condition of sustained and high-speed solar winds, especially for the southward directed solar wind at the dayside of the Earth's magnetosphere, which are easily transferring energies from the solar wind to the magnetosphere. Therefore, the geomagnetic storms are usually associated with CMEs (Gosling, 1993; Lakhina and Tsurutani, 2016). On the other hand, a recent work suggested that the large solar flare has also major impacts on the Earth's magnetosphere, but the relationship between solar flare radiation and geomagnetic storms are rarely studied (Liu J et al., 2021), the relationship will be helpful for forecasting space weather, since solar flares are much easier to observe. Using the newly-launched satellite, the Macau Science Satellite-1 (MSS-1, Zhang K, 2023), we investigated the Sun–Earth relationship between the solar flare radiation and geomagnetic storms during October 1–12, 2024.

2. Observations

MSS-1 is a low-inclination geomagnetic satellite project, which includes two satellites: MSS-1A and MSS-1B. MSS-1A aims to measure magnetic fields of the Earth with an unprecedented accuracy, and it is equipped with the Coupled Dark State Magnetometer (CDSM), the vector magnetometer of Flux Gate Magnetometer (FGM), the Energetic Electron Spectrometer (EES), the Vector Field Magnetometer (VFM), the micro Advanced Stellar Compass (ASC), the GNSS receiver subsystem, and the Satellite Laser Ranging (SLR). CDSM is a reference instrument that ensures the instantaneous calibration of magnetic fields; FGM can measure the geomagnetic field of the South Atlantic geomagnetic anomal; ESS is used to measure the energetic electron flux between 50 keV and 2.0 MeV; and VFM is designed for measuring the vector magnetic field of the Earth. ASC is a star tracker system; GNSS can provide the satellite's position, speed and time information; and SLR is a satellite orbit measurement technology. MSS-1B composes of the Energetic Electron Spectrometer (EES) and the solar X-ray detector (SXD), which is mainly used for monitoring solar activities and their effect to the interplanetary space. SXD aims to detect the solar X-ray spectrum in the energy range of about 0.02–12 Å (1–600 keV), and it consists of the SXR detection unit (SXDU) and the HXR detection unit (HXDU). The time cadence is as high as 1 s (Shi YQ et al., 2023). In this study, the SXR irradiation between 0.5–10 Å and the vector magnetic fields are used.

The Geostationary Operational Environmental Satellite (GOES) is designed for monitoring solar actives. One payload named as the X-ray Sensor (XRS) is used to record solar SXR radiation at 1–8 and 0.5–4 Å with a high time cadence of 1 s. Another payload, which is named as the Space Environment In Situ Suite (SEISS), is used to detect the energy electrons and protons, especially for the high energy protons above 10 MeV. The Extreme ultraviolet Variability Experiment (EVE) on board the Solar Dynamics Observatory (SDO) mission measures the solar soft X-ray (SXR) and extreme ultraviolet (EUV) irradiance with high spectral resolution and temporal cadence. Here, the level 4 spectral and level 2B line products were used, which consists of the SXR/EUV spectrum and the Ly*α* irradiance at a temporal cadence of 1 minute, respectively.

The satellite WIND is mainly used to measure vector magnetic fields and plasma conditions in the interplanetary space. In this study, the products of WI_H0_MFI and OMNI2_H0_MRG1HR were used. The former was the interplanetary magnetic fields (IMFs) with a temporal cadence of 1 minute in the geocentric solar magnetospheric (GSM) coordinate, while the latter was the OMNI combined IMF and plasma data with a temporal cadence of 1 hour. Here, the 1-hour data is used because it releases earlier, and it fully meets our need, i.e., the long-time evolution of plasma data.

The three-hour *Kp* index (Matzka et al., 2021) is a planetary geomagnetic disturbance index, which is mainly used for monitoring the geomagnetic activity. According to the NOAA Space Weather Scale (https://www.swpc.noaa.gov/noaa-scales-explanation), the geomagnetic storm is divided into five scales: G1 (Kp = 5), G2 (Kp = 6), G3 (Kp = 7), G4 (Kp = 8, 9-), and G5 (Kp = 9), and they are described as minor, moderate, strong, severe, and extreme, respectively. The real-time Disturbance Storm-Time (*Dst*) index is often applied for characterizing the magnitude of geomagnetic storms, regarding as an indicator of disturbances in the Earth's magnetic field. It is provided by the World Data Center (WDC) for Geomagnetism, Kyoto.

3. Measurements

During October 1–12 2024, a significant number of solar flares occurred, including 6 X-class and 38 M-class flares. This analysis focuses on X-class flares due to their higher energy impact and associated space weather implications. Meanwhile, two groups of geomagnetic storms were triggered during October 6–8 and 10–12, respectively. Figure 1 shows the light curves of solar flares and the associated SEPs in multiple wavebands. Panel (a) presents the SXR fluxes recorded by GOES at 1–8 Å and 0.5–4 Å from October 1 to October 13, 2024. A number of solar flares can be clearly seen in the GOES light curve. The peak flux of six flares in GOES 1–8 Å exceeds a threshold of 10^{-4} W m^{-2}, regarded as the X-class or powerful flares, as outlined by the blue horizontal line. According to their effects on geomagnetic field, i.e., two groups of geomagnetic storms, we divide the flares into two groups: LSFs1 containing the X7.1 and X9.0 flares and LSFs2 containing the X2.2, X1.0, X1.8 and X1.4 flares. Table 1 lists some key parameters of these powerful flares. They are all associated with CMEs. Panel (b) shows the normalized SXR fluxes measured by MSS-1B/SXDU at 1–10 Å and 0.5–1 Å. Here, the time resolution has been interpolated into 1 minutes, and thus the light curves have a high signal-to-noise ratio (Li D et al., 2024b; Li JP et al., 2025). Most of the powerful flares were detected by MSS-1B/SXDU, and they appear to match the GOES fluxes. However, some flares were not consistent well with the GOES flares, e.g., the X9.0 flare. This is because MSS-1 is a low-inclination satellite, and it has observational night for the Sun. Panel (c) gives the XUV and EUV light curves measured by SDO/EVE at 1–300 Å and 300–1060 Å, as well as the Ly*α* band at 1210–1220 Å. Corresponding peaks appear revealing strong XUV, EUV and Ly*α* radiation during the 6 flares. Panel (d) shows the high-energy proton fluxes observed by GOES/SEISS. The proton flux >10 MeV was much greater than the SWPC 10 MeV warning threshold during October 9–11, which could be regarded as a strong SEP event. There was no SEP event during October 3–6.

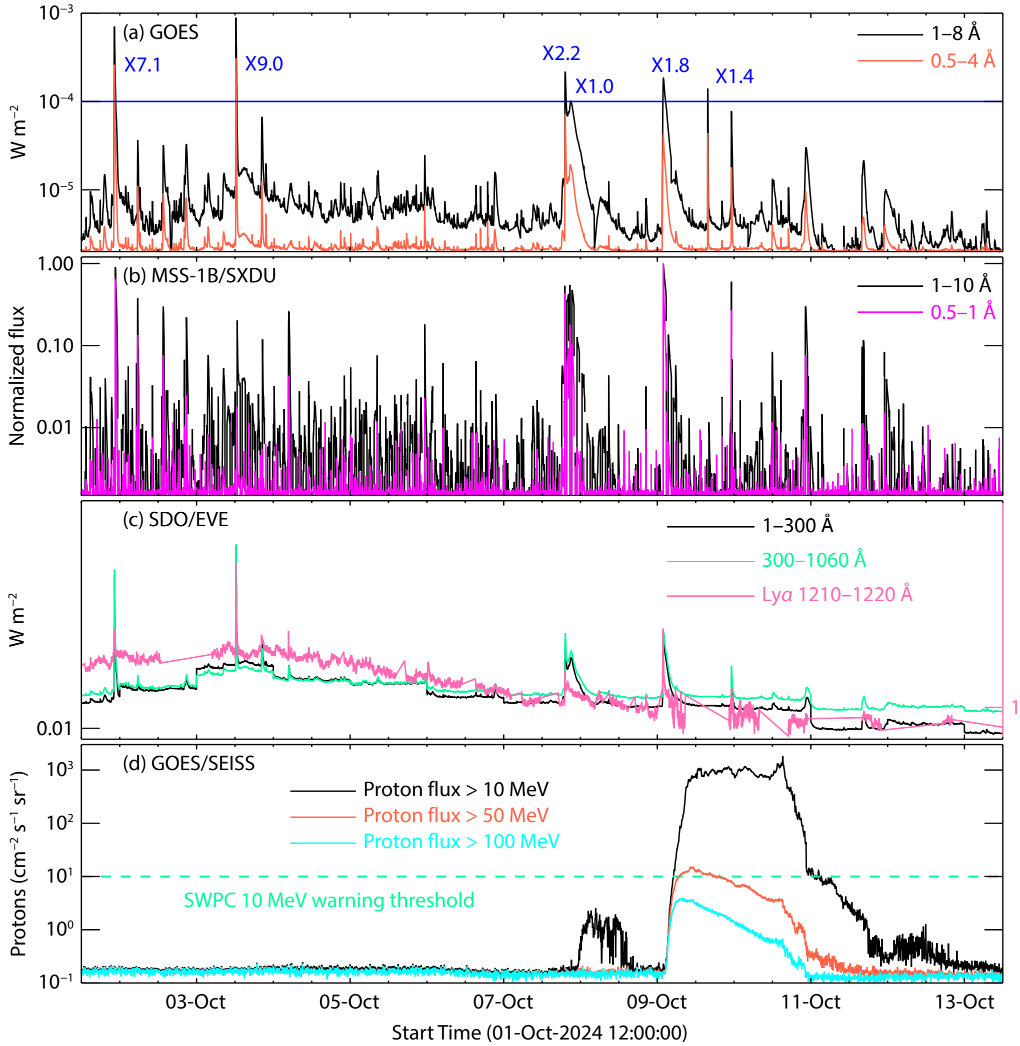

Figure 1. Solar flares and SEPs. (a) SXR fluxes recorded by GOES at 1–8 Å and 0.5–4 Å. (b) SXR light curves measured by MSS-1B/SXDU at 1–10 Å and 0.5–1 Å. (c) XUV and EUV fluxes observed by SDO/EVE at 1–300 Å, 300–1060 Å, and 1210–1220 Å. (d) Fluxes of high-energy protons derived from GOES/SEISS.

Table 1. The powerful flares observed during October 1–12 2024.

Date	Class	Time (UT)[a]			Position[b]	
		Start	Peak	Stop	Solar-X	Solar-Y
20241001	X7.1	21:58	22:20	22:29	−255″	−367″
20241003	X9.0	12:08	12:18	12:27	49″	−354″
20241007	X2.2	19:02	19:13	19:30	816″	−311″
20241007	X1.0	19:50	21:02	00:00	921″	−268″
20241009	X1.8	01:25	01:56	02:14	131″	114″
20241009	X1.4	15:44	15:47	15:53	939″	−178″

[a]The time is automatically provided by the GOES team;
[b]The position is calculated from the SDO/AIA observation (cf. Li D et al., 2024a).

Figure 2a presents the magnetic residual fields due to the magnetospheric current systems, which were measured by MSS-1A/VFM, they are the radial (B_r), colatitude (B_θ), and longitude (B_ϕ) components of the geomagnetic fields. The total geomagnetic fields (B_t) are also given by integrating over the three components of vector magnetic fields (i.e., $B_t = (B_r^2 + B_\phi^2 + B_\theta^2)^{1/2}$). They have been corrected by removing the core and crustal fields that were predicted by the CHAOS-7 geomagnetic field model (Finlay et al., 2020), and the ionospheric field as predicted by the CM6 geomagnetic field model (Sabaka et al., 2020). Thus, they can represent

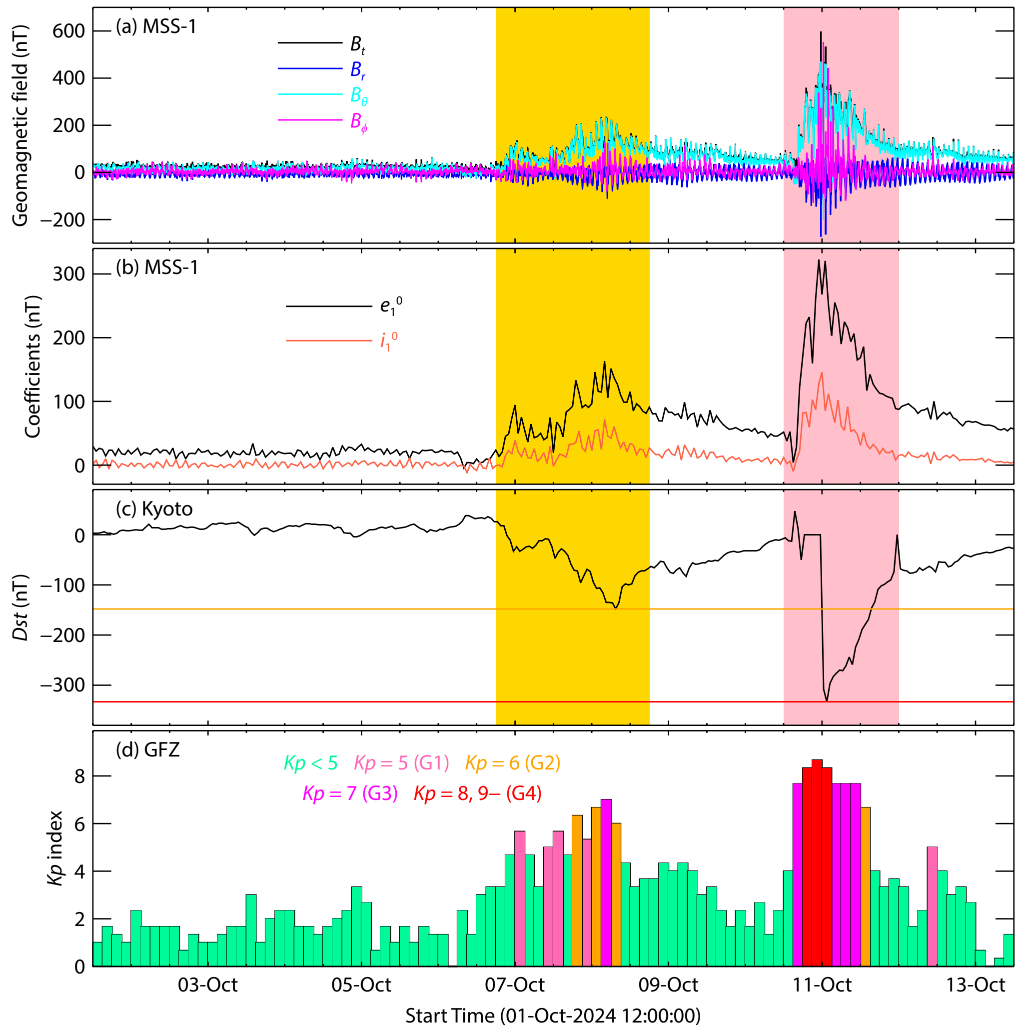

Figure 2. Geomagnetic indices. (a) Time series of the corrected magnetic fields in the geomagnetic coordinate system. (b) Time series of the magnetospheric external (e_1^0) and induced (i_1^0) coefficients. (c) The geomagnetic indices *Dst* from WDC. (d) The geomagnetic *Kp* index from GFZ Potsdam.

the disturbed magnetic fields due to geomagnetic storms.

The geomagnetic fields reveal two evidently disturbances, which could be regarded as two groups of geomagnetic storms, as highlighted by the gold and pink shadows. One storm that was occurred in October 6–8 is a bit weaker, and another occurred in October 10–12 is stronger. Panel (b) shows the time series of the external (e_1^0) and induced (i_1^0) coefficients that were estimated from the residual magnetic fields (Yao HB et al., 2023; Yan Q and Yao HB, 2024). The external coefficient is bigger than 100 nT on October 8, and it jumps up to 300 nT on October 11. Conversely, the induced coefficient is much smaller. Panel (c) shows the real-time *Dst* index that was derived from geomagnetic observatory data. The *Dst* index dips to −148 nT on October 8, and it jumps down to −300 nT with a minimum value of −333 nT on October 11, indicating intense geomagnetic storms. It is interesting that the *Dst* index is consistent with the external coefficient derived from the MSS-1 data, suggesting that the external coefficient rather than the induced coefficient could represent the geomagnetic signal that is associated with the geomagnetic storm. In order to characterize the magnitude of geomagnetic storms, we plot the time evolution of the *Kp* index, as shown in panel (d). The geomagnetic storm level is G3 (magneton) on October 8, regarding as a strong geomagnetic storm. While it could be G4 (red) on October 11, suggesting a severe geomagnetic storm.

In order to establish a connection between solar flares and geomagnetic storms in the interplanetary space, Figure 3 presents the interplanetary magnetic field (IMF) and solar wind parameters. Panels (a) and (b) show the time evolution of IMF parameters, including the total magnetic field B_t, the southward magnetic component B_z, and the azimuthal magnetic components B_x, B_y in the GSM coordinate. All IMF parameters exhibited two distinct types of disturbances. The southward magnetic component of the IMF dropped to about −10 nT during October 6–8, and it could plunge to −43 nT during October 10–12, as indicated by the gold an pink highlights. Panel (c) shows the plasma temperature and the ion number density. They revealed a weak fluctuation during October 6–8, but a strong fluctuation during October 10–12. Panel (d) plots the plasma flow speeds, i.e., the velocity of solar winds. The solar wind speed increased to about 500 km s^{-1} during October 6–8, and it could reach to be as high as about 800 km s^{-1} during October 10–12. The IMF and solar wind parameters agreed with the disturbances of geomagnetic fields on the Earth.

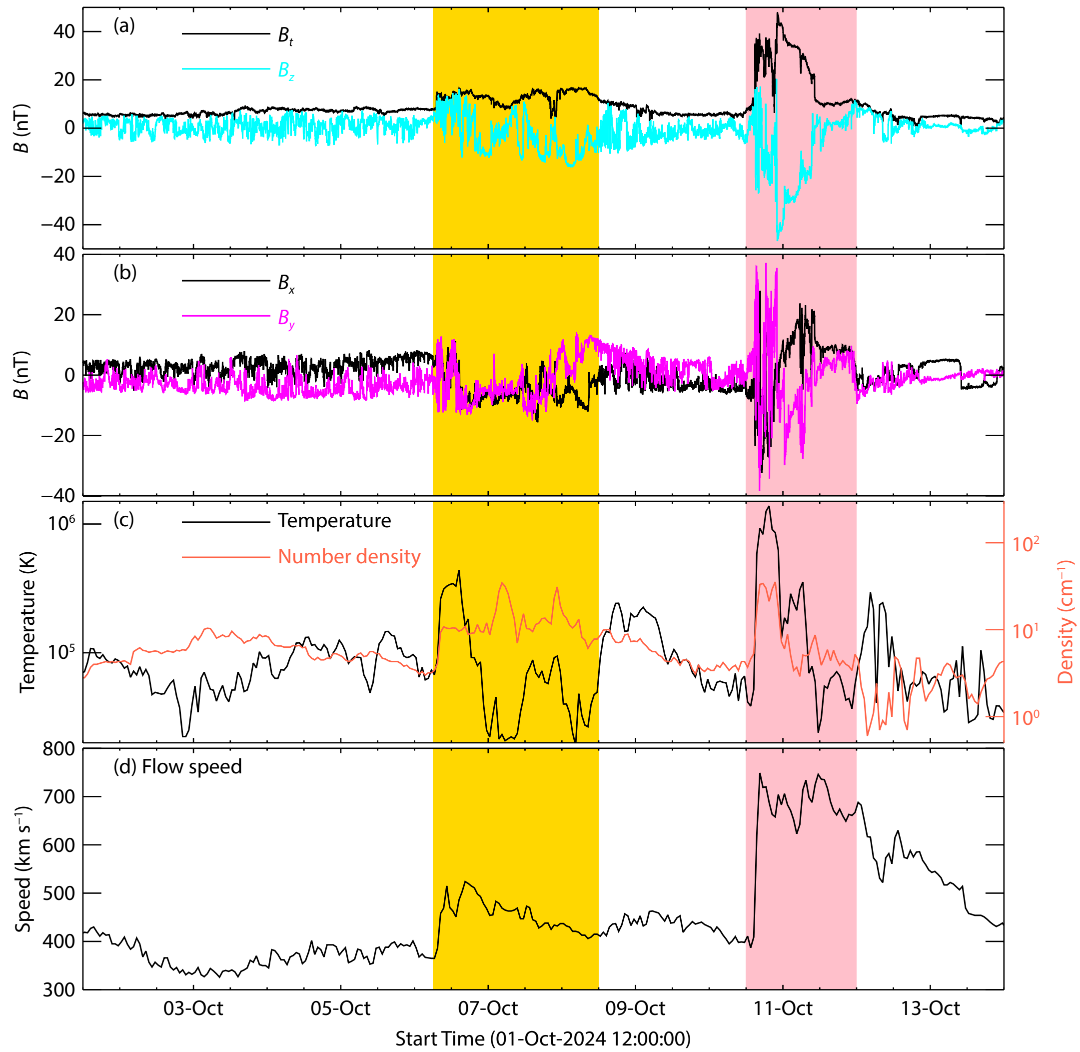

Figure 3. Interplanetary magnetic field (IMF) and solar wind parameters. (a) and (b) Time series of IMF parameters, such as the total magnetic field B_t, the southward magnetic component B_z, and the azimuthal magnetic components B_x, B_y in the GSM coordinate. (c) and (d) Time seise of the plasma temperature, the ion number density, and the plasma flow speed.

LSFs1, which contains two largest flares, corresponds a strong geomagnetic storm (G3), but LSFs2 corresponds a severe geomagnetic storm (G4). To illustrate it, we estimate the radiated energy (E_λ) in multiple wavebands during the large flares. Both GOES and SDO/EVE record the solar irradiance that comes from the entire Sun, which contains the background emission besides the flare radiation. To calculate the radiated energy (E_λ) of solar flares in the specific waveband (λ), we can integrate over the background-subtracted irradiance ($I_{ob} - I_{bk}$) of the solar flare (c.f. Emslie et al., 2012; Zhang QM et al., 2019; 2023; Li D et al., 2023), as shown in Equation (1):

$$E_\lambda = 2\pi d^2 \int_{t_0}^{t_1} (I_{ob}(t) - I_{bk}(t))\,\mathrm{d}t. \tag{1}$$

Here, d is equal to 1 AU, representing the distance between the Sun and the Earth. t_0 and t_1 denote to the onset and end time of the solar flare. I_{ob} and I_{bk} are the observed and background irradiance, respectively. t_0 is roughly equal to the start time in Table 1, but t_1 is apparent different from the stop time in Table 1, mainly due to the various flare eruptions in the SXR flux. Therefore, t_1 is defined as the flare irradiance decreases to the valley value, as marked by the magenta vertical lines in Figure 4. The background irradiance (I_{bk}) is a bit complicated due to the long time interval in our case, since we wanted to obtain the background irradiance during October 1–12. We first removed the flare radiation (i.e., C, M and X flares) from the observed irradiance, referred as the flare-removed flux. Then, the background irradiance could be determined by a 1-day (1440 minutes) running average for the flare-removed flux, as indicated by the tomato curve in Figure 4, and they appear to match the background irradiance. We also tried some other windows (i.e., 2-, 3-, or 5-days) to estimate the background irradiance, and they had slightly affected the estimation of the radiated energy, i.e., roughly 1%. So, it hardly influences the magnitude of the estimated energy.

Figure 4 presents the time series of radiated power in wavebands of SXR (1–8 Å), XUV (1–300 Å) and EUV (300–1060 Å). Noting that the X2.2 and X1.0 flares are very close in the light curve, for instance, the X2.2 flare does not decrease to its valley value when the X1.0 flare begins. So, they are regarded as one flare with a

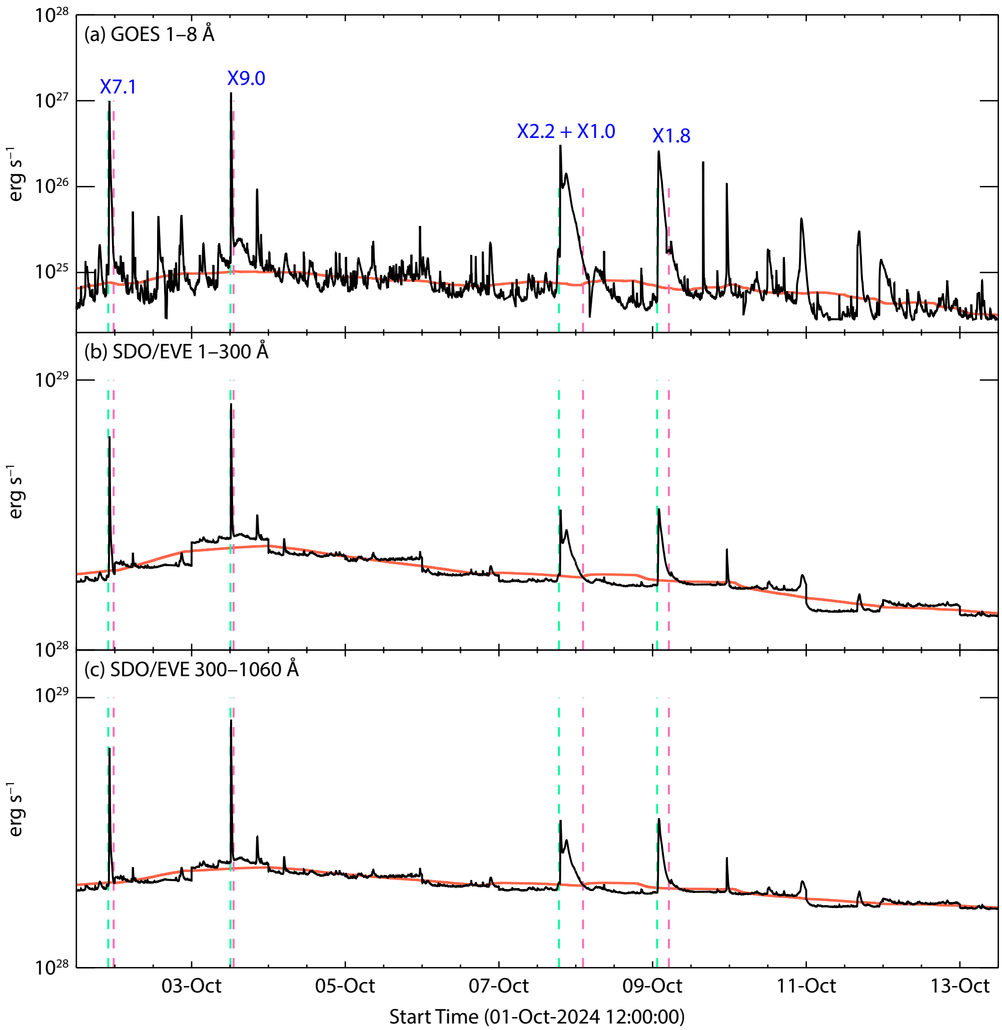

Figure 4. Energy estimation of solar flares in wavebands of SXR, XUV, and EUV. The tomato curve represents the background irradiance in each waveband. The vertical dashed lines mark the onset (t_0) and end (t_1) time of the energy estimation.

long time duration. Also the X1.4 flare does not detect by SDO/EVE, and we did not consider it. At last, the radiated energy of four powerful flares is estimated, as listed in Table 2. We can note that the radiated energy of the X2.2 and X1.8 flares is larger than that of the X7.1 and X9.0 flares, for instance, two or three times larger in wavebands of XUV and EUV. Conversely, they are roughly equal in the waveband of SXR.

4. Conclusion and Discussion

It is well accepted that geomagnetic storms are the results of impact of interplanetary disturbances brought about by CMEs and the interplanetary solar wind. Southward magnetic component in the interplanetary disturbances plays a crucial role. (e.g., de Lucas et al., 2007; Gonzalez et al., 2001; Lakhina et al., 2004; Chi YT et al., 2016; Meng X et al., 2019). Solar flares serve as the ultimate sources of geomagnetic storms, and the investigation of their connection constitutes a kind of end-to-end study. This kind of study is worthwhile since flare observation is relatively easy, however, such a kind of investigations are still insufficient (cf. Liu J et al., 2021). With the combined observational data measured by MSS-1, GOES, and SDO/EVE, we explored the relationship between powerful flares and geomagnetic storms in October of 2024. Two powerful flares in October 1–3 corresponded a strong geomagnetic storm (G3) during October 6–8, but they did not produce the SEP event. On the contrary, four less powerful flares

Table 2. Energy estimation of the powerful flares.

Flare	t_0 (UT)	t_1 (UT)	E_{SXR} (10^{30} erg)	E_{XUV} (10^{31} erg)	E_{EUV} (10^{31} erg)
X7.1	21:58	23:39	1.06	4.79	5.31
X9.0	12:08	13:07	0.84	5.33	5.26
X2.2 + X1.0	19:02	02:17	1.80	11.8	12.4
X1.8	01:25	05:06	1.03	7.73	8.11

in October 7–9 triggered a severe geomagnetic storm (G4) during October 10–12, and they produced a strong SEP event during October 9–11. The two geomagnetic storms were both observed by MSS-1A/VFM. The corrected geomagnetic fields, which have been removed the core, crustal, and ionospheric fields, show obviously disturbed magnetic fields. We show that the external (e_1^0) coefficient (Yao HB et al., 2023), which is calculated from the observed geomagnetic field, is consistent well with the *Dst* index, demonstrating that the magnetic fields measured by MSS-1 can well be used for monitoring the geomagnetic disturbance (Yan Q and Yao HB, 2024).

Using the in-situ measurement from the WIND spacecraft, the IMF and solar wind parameters are extracted to connect the powerful flares and geomagnetic storms in the interplanetary space. The interplanetary magnetic fields showed significant disturbance during October 6–8 and 10–12. Moreover, the southward magnetic component also revealed obvious variation, for instance, it was a bit weak (−10 nT) in October 6–8 but could be very strong (−43 nT) in October 10–12, indicating that the influence of solar flares was toward to the Earth. The physical parameters such as plasma temperature and ion density in the interplanetary space showed significant disturbances during the same time interval. At last, the speed of solar wind appeared to increase quickly, for instance, it was about 500 km s^{-1} during October 6–8 and could be about 800 km s^{-1} during October 10–12. Those observational facts suggest that the IMF and solar wind parameters were highly associated with the two geomagnetic storms on the Earth.

Typically, a solar flare has effects on the Earth, although the effects may not always be direct. In our case, the IMF and solar wind parameters and geomagnetic storms matched well with each other. However, the correspondence between solar flares and geomagnetic storms was a bit complex. The two strong flares (i.e., X7.1 and X9.0) corresponded the strong geomagnetic storm, while the other less stronger flares (i.e., X2.2, X1.0, X1.8) have induced the severe geomagnetic storm. Then, the radiated energy of powerful flares were estimated in wavebands of SXR, XUV, and EUV. The radiated energies in the SXR channel were similar for these powerful flares, but they were clearly different in wavebands of XUV and EUV. The radiated energy of LSFs2 was much bigger than that of LSFs1, implying that the heavy geomagnetic storm was more associated with the radiated energy rather than the class level of solar flares. This is reasonable, because the class level is only determined by the peak flux of SXR radiation. The radiated energy of large solar flares also matched the IMF and solar wind parameters in interplanetary space. The idea is that the larger energy of LSFs2 triggered the stronger IMF and faster solar wind and further caused the severe geomagnetic storm, while the smaller energy of LSFs1 only induced the weaker IMF and slower solar wind. Therefore, the time lag between LSFs1 and the strong storm was much longer than that between LSFs2 and the severe storm. The disturbances in IMF and solar wind parameters linking powerful solar flares to geomagnetic storms also suggest that the strong geomagnetic storm is a typical effect from CMEs rather than solar flares. That is, solar flares are not the direct cause of geomagnetic storms. However, the intensity of these geomagnetic storms is very consistent with the energy of the flares, indicating that the CMEs that erupted during these flares are closely related to the flares.

The radiated energy in the EUV waveband of LSFs2 is much bigger than that of LSFs1 also suggests that the EUV irradiance of large solar flares may play a major role in its association with the severe geomagnetic storm, which is similar to pervious findings (e.g., Sastri and Murthy, 1975; Curto, 2020). It should be pointed out that the simple relationship between large solar flares and geomagnetic storms is built on the foundation that the large solar flare can firstly disturb the southward magnetic field and accelerate the solar wind in the interplanetary space, which is regarded as the Sun–Earth bridge (e.g., de Lucas et al., 2007; Lakhina and Tsurutani, 2016). This is because that the magnetosphere of the Earth is the outermost layer of the geo-space system that deflects energetic ions from the Sun. Also, total irradiance of a solar flare is proportional to its duration, the more total irradiance usually means the longer duration. A long-duration flare is typically associated with a CME that can cause sustained disturbance to interplanetary space, especially when the flare is very large. Finally, we should stress that this is the preliminary conclusion. In the future, the large-sample statistical research will be done when MSS-1 accumulating sufficient observational data.

Open Research Section

Publicly available data sets were analyzed in this study. They can be found here: https://mss.must.edu.mo/, https://kp.gfz-potsdam.de/en/data, https://cdaweb.gsfc.nasa.gov/index.html, https://www.ngdc.noaa.gov/stp/satellite/goes-r.html, https://lasp.colorado.edu/eve/data_access/eve-space-weather/index.html, https://wdc.kugi.kyoto-u.ac.jp/dst_realtime/index.html.

Acknowledgments

This work is funded by NSFC under grants 12250014, 42250101 and 12403068. It is also supported by youth funding of Jiangsu province BK20241707. The work is especially supported by the Macao Foundation. H. Ji thanks Xinjiang Uygur Autonomous Region for the support through “Tianchi Talent” special expert project. We thank the teams of MSS-1, GOES, WIND, and SDO/EVE for their open data use policy. We also thank the geomagnetic observatories (Kakioka [JMA], Honolulu and San Juan [USGS], Hermanus [RSA], Alibag [IIG]), NiCT, INTERMAGNET, and many others for their cooperation to make the real-time (quicklook) *Dst* index available.

References

Benz, A. O. (2017). Flare observations. *Living Rev. Sol. Phys.*, *14*(1), 2. https://doi.org/10.1007/s41116-016-0004-3

Chi, Y. T., Shen, C. L., Wang, Y. M., Xu, M. J., Ye, P. Z., and Wang, S. (2016). Statistical study of the interplanetary coronal mass ejections from 1995 to 2015. *Sol. Phys.*, *291*(8), 2419–2439. https://doi.org/10.1007/s11207-016-0971-5

Cliver, E. W., and Svalgaard, L. (2004). The 1859 solar-terrestrial disturbance and the current limits of extreme space weather activity. *Sol. Phys.*, *224*(1–2), 407–422. https://doi.org/10.1007/s11207-005-4980-z

Curto, J. J. (2020). Geomagnetic solar flare effects: a review. *J. Space We. Space Climate*, *10*, 27. https://doi.org/10.1051/swsc/2020027

de Lucas, A., Gonzalez, W. D., Echer, E., Guarnieri, F. L., Dal Lago, A., da Silva, M.

R., Vieira, L. E. A., and Schuch, N. J. (2007). Energy balance during intense and super-intense magnetic storms using an Akasofu ε parameter corrected by the solar wind dynamic pressure. *J. Atmos. Sol-Terr. Phys.*, *69*(15), 1851–1863. https://doi.org/10.1016/j.jastp.2007.09.001

Emslie, A. G., Dennis, B. R., Shih, A. Y., Chamberlin, P. C., Mewaldt, R. A., Moore, C. S., Share, G. H., Vourlidas, A., and Welsch, B. T. (2012). Global energetics of thirty-eight large solar eruptive events. *Astrophys. J.*, *759*(1), 71. https://doi.org/10.1088/0004-637X/759/1/71

Finlay, C. C., Kloss, C., Olsen, N., Hammer, M. D., Tøffner-Clausen, L., Grayver, A., and Kuvshinov, A. (2020). The CHAOS-7 geomagnetic field model and observed changes in the South Atlantic Anomaly. *Earth Planets Space*, *72*(1), 156. https://doi.org/10.1186/s40623-020-01252-9

Gonzalez, W. D., Joselyn, J. A., Kamide, Y., Kroehl, H. W., Rostoker, G., Tsurutani, B. T., and Vasyliunas, V. M. (1994). What is a geomagnetic storm?. *J. Geophys. Res.: Space Phys.*, *99*(A4), 5771–5792. https://doi.org/10.1029/93JA02867

Gonzalez, W. D., de Gonzalez, A. L. C., Sobral, J. H. A., Dal Lago, A., and Vieira, L. E. (2001). Solar and interplanetary causes of very intense geomagnetic storms. *J. Atmos. Sol-Terr. Phys.*, *63*(5), 403–412. https://doi.org/10.1016/S1364-6826(00)00168-1

Gosling, J. T. (1993). The solar flare myth. *J. Geophys. Res.: Space Phys.*, *98*(A11), 18937–18949. https://doi.org/10.1029/93JA01896

Hayakawa, H., Hattori, K., Pevtsov, A. A., Ebihara, Y., Shea, M. A., McCracken, K. G., Daglis, I. A., Bhaskar, A. T., Ribeiro, P., and Knipp, D. J. (2021). The intensity and evolution of the extreme solar and geomagnetic storms in 1938 January. *Astrophys. J.*, *909*(2), 197. https://doi.org/10.3847/1538-4357/abc427

Lakhina, G. S., Alex, S., Tsurutani, B. T., and Gonzalez, W. D. (2004). Research on historical records of geomagnetic storms. In *Proceedings of the International Astronomical Union* (pp. 3-15). Cambridge: Cambridge University Press. https://doi.org/10.1017/S1743921305000074

Lakhina, G. S., and Tsurutani, B. T. (2016). Geomagnetic storms: historical perspective to modern view. *Geosci. Lett.*, *3*(1), 5. https://doi.org/10.1186/s40562-016-0037-4

Li, D., Warmuth, A., Lu, L., and Ning, Z. J. (2021). An investigation of flare emissions at multiple wavelengths. *Res. Astron. Astrophys.*, *21*(3), 066. https://doi.org/10.1088/1674-4527/21/3/66

Li, D., Warmuth, A., Wang, J. C., Zhao, H. S., Lu, L., Zhang, Q. M., Dresing, N., Vainio, R., Palmroos, C., … Dominique, M. (2023). Global energetics of solar powerful events on 2017 September 6. *Res. Astron. Astrophys.*, *23*(9), 095017. https://doi.org/10.1088/1674-4527/acd592

Li, D., Dong, H. Y., Chen, W., Su, Y., Huang, Y., and Ning, Z. J. (2024a). A statistical investigation of the NEUPERT effect in solar flares observed with ASO-S/HXI. *Sol. Phys.*, *299*(5), 57. https://doi.org/10.1007/s11207-024-02299-7

Li, D., Li, J. P., Shen, J. H., Song, Q. W., Ji, H. S., and Ning, Z. J. (2024b). Long-period energy releases during a C2.8 flare. *Astron. Astrophys.*, *690*, A39. https://doi.org/10.1051/0004-6361/202450622

Li, J. P., Yang, X., Li, D., Shen, J. H., Yang, L., Wang, Y., Li, L. S., Shi, Y. Q., and Ji, H. S. (2025). Diagnostics of temperature andblue-shifted velocity using soft X-ray spectra from the Macau Science Satellite-1. *Earth Planet. Phys.*, *9*(3), 740–751. https://doi.org/10.26464/epp2025036

Liu, J., Wang, W. B., Qian, L. Y., Lotko, W., Burns, A. G., Pham, K., Lu, G., Solomon, S. C., Liu, L. B., … Wilder, F. (2021). Solar flare effects in the Earth's magnetosphere. *Nat. Phys.*, *17*(7), 807–812. https://doi.org/10.1038/s41567-021-01203-5

Lu, Z. K., Chen, F., Ding, M. D., Wang, C., Dai, Y., and Cheng, X. (2024). A model for heating the super-hot corona in solar active regions. *Nat. Astron.*, *8*(6), 706–715. https://doi.org/10.1038/s41550-024-02244-5

Matzka, J., Stolle, C., Yamazaki, Y., Bronkalla, O., and Morschhauser, A. (2021). The geomagnetic *Kp* index and derived indices of geomagnetic activity. *Space Wea.*, *19*(5), e2020SW002641. https://doi.org/10.1029/2020SW002641

Meng, X., Tsurutani, B. T., and Mannucci, A. J. (2019). The Solar and interplanetary causes of superstorms (minimum $Dst \leq$ -250 nT) during the space age. *J. Geophys. Res.: Space Phys.*, *124*(6), 3926–3948. https://doi.org/10.1029/2018JA026425

Priest, E. R., and Forbes, T. G. (2002). The magnetic nature of solar flares. *Astron. Astrophys. Rev.*, *10*(4), 313–377. https://doi.org/10.1007/s001590100013

Pulkkinen, A., Bernabeu, E., Thomson, A., Viljanen, A., Pirjola, R., Boteler, D., Eichner, J., Cilliers, P. J., Welling, D., … MacAlester, M. (2017). Geomagnetically induced currents: Science, engineering, and applications readiness. *Space Wea.*, *15*(7), 828–856. https://doi.org/10.1002/2016SW001501

Raouafi, N. E., Vourlidas, A., Zhang, Y. L., and Paxton, L. J. (2021). *Solar Physics and Solar Wind*. Washington: American Geophysical Union.

Sabaka, T. J., Tøffner-Clausen, L., Olsen, N., and Finlay, C. C. (2020). CM6: a comprehensive geomagnetic field model derived from both CHAMP and Swarm satellite observations. *Earth Planets Space*, *72*(1), 80. https://doi.org/10.1186/s40623-020-01210-5

Sastri, J. H., and Murthy, B. S. (1975). Geomagnetic effect associated with X-ray flare from Sco X-1. *Nature, 257*(5521), 35-36. https://doi.org/10.1038/257035a0

Shi, Y. Q., Li, L. S., Chen, J. W., Zuo, F. C., Zhang, X. P., Mei, Z. W., Wang, L., and Zhang, K. (2023). Design of the solar X-ray detector for the Macau Science Satellite-1B. *Earth Planet. Phys.*, *7*(1), 125–130. https://doi.org/10.26464/epp2023018

Warmuth, A., and Mann, G. (2016). Constraints on energy release in solar flares from RHESSI and GOES X-ray observations. I. Physical parameters and scalings. *Astron. Astrophys.*, *588*, A115. https://doi.org/10.1051/0004-6361/201527474

Yan, Q., and Yao, H. B. (2024). Recent geomagnetic storms observed by Macau Science Satellite-1. *Earth Planet. Phys.*, *8*(4), 565–569. https://doi.org/10.26464/epp2024047

Yan, X. L., Xue, Z. K., Jiang, C. W., Priest, E. R., Kliem, B., Yang, L. H., Wang, J. C., Kong, D. F., Song, Y. L., … Liu, Z. (2022). Fast plasmoid-mediated reconnection in a solar flare. *Nat. Commun.*, *13*(1), 640. https://doi.org/10.1038/s41467-022-28269-w

Yao, H. B., Ren, Z. Y., Pan, K. J., Tang, J. T., and Zhang, K. (2023). A global mantle conductivity model derived from 8 years of Swarm satellite magnetic data. *Earth Planet. Phys.*, *7*(1), 49–56. https://doi.org/10.26464/epp2023011

Zhang, K. (2023). A novel geomagnetic satellite constellation: Science and applications. *Earth Planet. Phys.*, *7*(1), 4–21. https://doi.org/10.26464/epp2023019

Zhang, Q. M., Cheng, J. X., Feng, L., Su, Y., Lu, L., Huang, Y., Li, D., Zhou, T. H., and Chen, J. L. (2019). Energy partition in two M-class circular-ribbon flares. *Astrophys. J.*, *883*(2), 124. https://doi.org/10.3847/1538-4357/ab3a52

Zhang, Q. M., Teng, W. L., Li, D., Dai, J., and Zhang, Y. J. (2023). Energetics of a solar flare and a coronal mass ejection generated by a hot channel eruption. *Astrophys. J.*, *958*(1), 85. https://doi.org/10.3847/1538-4357/ad05bc